

Preparation of PSFO and LPSFO nanofibers by electrospinning and their electronic transport and magnetic properties

Ying Su(苏影), Dong-Yang Zhu(朱东阳), Ting-Ting Zhang(张亭亭), Yu-Rui Zhang(张玉瑞), Wen-Peng Han(韩文鹏), Jun Zhang(张俊), Seeram Ramakrishna, and Yun-Ze Long(龙云泽)

Citation: Chin. Phys. B, 2022, 31 (**5**): 057305. DOI: 10.1088/1674-1056/ac3baa
Journal homepage: http://cpb.iphy.ac.cn; http://iopscience.iop.org/cpb

What follows is a list of articles you may be interested in

Research status and performance optimization of medium-temperature thermoelectric material SnTe

Pan-Pan Peng(彭盼盼), Chao Wang(王超), Lan-Wei Li(李岚伟), Shu-Yao Li(李淑瑶), and Yan-Qun Chen(陈艳群)
Chin. Phys. B, 2022, 31 (**4**): 047307. DOI: 10.1088/1674-1056/ac20c9

Magneto-transport properties of thin flakes of Weyl semiconductor tellurium

Nan Zhang(张南), Bin Cheng(程斌), Hui Li(李惠), Lin Li(李林), and Chang-Gan Zeng(曾长淦)
Chin. Phys. B, 2021, 30 (**8**): 087304. DOI: 10.1088/1674-1056/ac0a5e

Bound in continuum states and induced transparency in mesoscopic demultiplexer with two outputs

Z Labdouti, T Mrabti, A Mouadili, E H El Boudouti, F Fethi, and B Djafari-Rouhani
Chin. Phys. B, 2020, 29 (**12**): 127301. DOI: 10.1088/1674-1056/abad23

Electronic transport properties of Co cluster-decorated graphene

Chao-Yi Cai(蔡超逸), Jian-Hao Chen(陈剑豪)
Chin. Phys. B, 2018, 27 (**6**): 067304. DOI: 10.1088/1674-1056/27/6/067304

Electronic states and spin-filter effect in three-dimensional topological insulator Bi_2Se_3 nanoribbons

Genhua Liu(刘根华), Pingguo Xiao(肖平国), Piaorong Xu(徐飘荣), Huiying Zhou(周慧英), Guanghui Zhou(周光辉)
Chin. Phys. B, 2018, 27 (**1**): 017304. DOI: 10.1088/1674-1056/27/1/017304

Preparation of PSFO and LPSFO nanofibers by electrospinning and their electronic transport and magnetic properties

Ying Su(苏影)[1,†], Dong-Yang Zhu(朱东阳)[1,†], Ting-Ting Zhang(张亭亭)[1], Yu-Rui Zhang(张玉瑞)[1], Wen-Peng Han(韩文鹏)[1], Jun Zhang(张俊)[1], Seeram Ramakrishna[2], and Yun-Ze Long(龙云泽)[1,3,‡]

[1] *Collaborative Innovation Center for Nanomaterials & Devices, College of Physics, Qingdao University, Qingdao* 266071, *China*
[2] *Center for Nanofibers & Nanotechnology, Department of Mechanical Engineering, National University of Singapore, Singapore* 117574, *Singapore*
[3] *Collaborative Innovation Center for Eco-Textiles of Shandong Province, and State Key Laboratory of Bio-Fibers and Eco-Textiles, Qingdao University, Qingdao* 266071, *China*

(Received 23 September 2021; revised manuscript received 15 November 2021; accepted manuscript online 20 November 2021)

$Pr_{0.5}Sr_{0.5}FeO_3$ (PSFO) and $La_{0.25}Pr_{0.25}Sr_{0.5}FeO_3$ (LPSFO) nanofibers are prepared by electrospinning followed by calcination, and their morphologies, microstructures, electronic transports, and magnetic properties are studied systematically. The temperature-dependent resistance curves of PSFO and LPSFO nanofibers are measured in a temperature range from 300 K to 10 K. With the temperature lowering, the resistance increases gradually and then decreases sharply due to the occurrence of ferromagnetic metal phase. The metal–insulator transition temperatures are about 110 K and 180 K for PSFO and LPSFO nanofibers, respectively. The electronic conduction behavior above the transition temperature can be described by one-dimensional Mott's variable-range hopping (VRH) model. The hysteresis loops and the field-cooled (FC) and zero-field-cooled (ZFC) curves show that both PSFO nanofiber and LPSFO nanofiber exhibit ferromagnetism. Although the doping of La reduces the overall magnetization intensity of the material, it increases the ferromagnetic ratio of the system, which may improve the performance of LPSFO in solid oxide fuel cell.

Keywords: $Pr_{0.5}Sr_{0.5}FeO_3$, $La_{0.25}Pr_{0.25}Sr_{0.5}FeO_3$, electrospinning, electronic transport, magnetic properties

PACS: 73.63.–b, 75.75.–c, 81.07.–b, 81.05.Je **DOI:** 10.1088/1674-1056/ac3baa

1. Introduction

Solid oxide fuel cell (SOFC) has been extensively studied through a variety of methods to improve battery performance in the past two decades.[1–4] Compared with current commercial fuel cells, the SOFC possesses some outstanding features, which make it become a research hotspot. For example, it has higher current density and power density than other batteries,[5] the resistivity of the electrolyte is usually negligible, and in most cases, the battery performance mainly depends on the cathode loss.[6] For all-solid structure, the ceramic materials serve as electrolytes and electrodes, it solves the limitation in using precious metals as catalysts, and can directly use hydrogen, methane, and alcohol as fuels. Despite many advantages, the factors hindering the SOFC from bing commercialized are high cost and stability, resulting in its short service life.[7] The scientific community has made efforts to solve the problem and has made many achievements. In the past ten years, the theory and application of SOFC have been studied in more depth, and the battery performance has been continuously improved through various methods such as thin film formation technology, doping technology, and substitution of nanomaterials.[8–11] Nanomaterials and related nanotechnology, as one of the thin film forming technologies, have received more and more attention because they can improve battery performance by reducing the polarization resistance of the battery and generating new functions, thus significantly developing the current SOFC technology.[12–15]

The breakthroughs in the preparation methods and technologies of nanomaterials have brought more unique synergistic properties of nanomaterials, such as high stability, excellent electrical conductivity, large specific surface area, easy handling, excellent electrical and photochemical properties. Therefore, it has aroused great interest in scientific research and potential applications, especially widely used in energy conversion, storage, catalysis, and other energy sources.[16–18] Electrospinning has been widely used as a simple and efficient spinning process, which can make nanofibers from various polymer solutions. Compared with other preparation methods of nanomaterials, this technology has the advantages of low cost, simple and efficient preparation process, and easy control of fiber structure and size. The use of nanomaterials to replace traditional materials has significantly improved the performance of electronic and energy devices. For example, the performances of materials can be improved by optimizing and modifying materials such as solid oxide fuel cell cathodes, anodes, and electrolytes. Thus, the electrochemical efficiency of solid oxide fuel cells can be improved.[19–23]

The biggest limitation of traditional SOFC is that it is difficult to realize commercial application because of its high

[†] These two authors contributed equally to this work.
[‡] Corresponding author. E-mail: yunze.long@163.com; yunze.long@qdu.edu.cn
© 2022 Chinese Physical Society and IOP Publishing Ltd

operating temperature. However, the operating characteristics of proton-conducting solid oxide fuel cells (H-SOFC) that can be used at lower temperatures have attracted more and more attention of scientists.[24–28] Moreover, studies have shown that doping and modification of traditional cathode materials can greatly improve the electrochemical performances of H-SOFC cathodes.[29–33] For example, Sr-doped $LaFeO_3$ cathode can improve the fuel cell performance.[34–36] In addition, the Sr-doped $LaFeO_3$ cathode is doped with Pr element, which improves the hydration capacity in the electrolyte material and the cathode material, and has the potential for proton migration.[37,38] The $Pr_{0.5}Sr_{0.5}FeO_3$ and $La_{0.25}Pr_{0.25}Sr_{0.5}FeO_3$ were used as the cathode materials of low-temperature SOFCs, which significantly improve the electrochemical efficiency of SOFCs. Moreover, studies have shown that PSFO and LPSFO nanofibers prepared by electrospinning exhibit better electrochemical performances than granular PSFO and LPSFO.[39]

The study of the physical properties of such materials is conducive to the in-depth understanding of the electronic transport, magnetic properties, and reaction mechanisms inside the materials, thereby facilitating the exploration of material applications and the improvement of performance. In 1999, Nowik and Awana studied and analyzed the magnetic properties of macroscopic $PrSr_2Fe_3O_{9-\delta}$ ($\delta < 0.1$).[40] They tested the hysteresis loop under the magnetic field range from -1.5 T to 2 T at the temperature of 5 K, and also measured the field-cooled (FC) and zero-field-cooled (ZFC) curve under the magnetic field of 20 Oe (1 Oe = 79.5775 $A{\cdot}m^{-1}$) at a temperature between 5 K and 300 K. As result, the phase transition temperature point was obtained to be 190 K.[40] In 2014, Zhu *et al.* studied the magnetic properties of PSFO bulk materials. They measured the FC and ZFC curves of the sample under a magnetic field of 1000 Oe at the temperature between 10 K and 300 K, and analyzed the dependence of Young's modulus on temperature. The properties confirm the existence and influence of the magnetic spin glass transition.[41] Furthermore, Chen *et al.* also studied the relationship between the specific heat capacity and the temperature of La bulk materials, the FC and ZFC curves were obtained under a magnetic field of 1000 Oe in a temperature range from 10 K to 300 K. Through mutual verification of phase change and specific heat capacity, the ordered transitions of charges in $(La_{1-x}Pr_x)_{1/3}Sr_{2/3}FeO_{3-\delta}$ bulk materials were analyzed.[42] Previous work provides a good theoretical basis for the research of fiber materials. However, there have been few studies on the physical properties of PSFO and LPSFO nanofibers. Therefore, the further understanding of the electronic transport and magnetic properties of PSFO nanofibers and LPSFO nanofibers have far-reaching significance for their applications in energy devices.

In this work, we systematically study the electronic transport and magnetic properties of PSFO and LPSFO nanofibers. First, we prepare one-dimensional (1D) nanofibers PSFO/PVP and LPSFO/PVP by using the electrospinning method, and also prepare the pure phase inorganic nanofibers $Pr_{.5}Sr_{0.5}FeO_3$ and $La_{0.25}Pr_{0.25}Sr_{0.5}FeO_3$ by the post-processing methods such as calcination. Then, the structure and electronic transport and magnetic properties of PSFO and LPSFO are systematically studied. We find that the properties of PSFO show some differences in our work. The ratio of ferromagnetism is obviously reduced, and it shows obvious ferromagnetic properties after having been doped. The phenomenon can be attributed to the influence of nanostructure on macroscopic properties.

2. Experimental details

2.1. Materials

The $Fe(NO_3)_3{\cdot}9H_2O$ ($\geq$ 98.5%), $La(NO_3)_3{\cdot}nH_2O$ ($\geq$ 44.0%), $Sr(NO_3)_2$ ($\geq$ 99.5%), dimethylformamide (DMF), $PrN_3O_9.6H_2O$ (99.9%), and polyvinyl pyrrolidone (PVP, $M_W \approx 9.0 \times 10^5$) were obtained from Aladdin Biochemical Technology Co., Ltd. All chemicals were purchased and used directly without further purification.

2.2. Preparation of $Pr_{0.5}Sr_{0.5}FeO_3$ and $La_{0.25}Pr_{0.25}Sr_{0.5}FeO_3$ nanofibers

The PSFO and LPSFO nanofibers were prepared by the electrospinning method followed by the calcination.

Firstly, the precursor solution of PSFO and LPSFO should be prepared.

(i) PSFO precursor solution preparation

Firstly, 0.436 g $PrN_3O_9{\cdot}6H_2O$, 0.212-g $Sr(NO_3)_2$, 0.808-g $Fe(NO_3)_3{\cdot}9H_2O$, and 10-g DMF solvents were mixed. Then, the $Pr_{0.5}Sr_{0.5}FeO_3$ inorganic salt solution was obtained by magnetic stirring for 6 h. Finally, 1.5-g PVP was added into the above-mentioned inorganic salt solution and magnetically stirred for 12 h to obtain the required precursor solution.

(ii) LPSFO precursor solution preparation

Similar to the above steps, mixing 0.18-g $La(NO_3)_3 \cdot nH_2O$, 0.11-g $PrN_3O_9{\cdot}6H_2O$, 0.106-g $Sr(NO_3)_2$, 0.41-g $Fe(NO_3)_3{\cdot}9H_2O$, and 10-g DMF and magnetically stirred for 6 h to obtain a well-mixed $La_{0.25}Pr_{0.25}Sr_{0.5}FeO_3$ inorganic salt solution. Then, 1.5-g PVP was added into the above-mentioned inorganic salt solution, and the required precursor solution was obtained by magnetic stirring for 12 h.

The precursor solutions of PSFO and LPSFO obtained by the above configuration were electrospun separately. Take an appropriate amount of solution and poured it into a syringe with a metal needle, then placed the syringe on a portable spinning machine. The working voltage was set to be 18 kV, the working distance was 18 cm, and the solution flow rate

was set to be 1 ml·h^{-1}. After being spun for several hours, the PSFO/PVP and LPSFO/PVP nanofiber membranes were obtained. Then, the organic/inorganic hybrid nanofiber membranes were placed in the ceramic ark, and calcined in a high-temperature vacuum tube furnace. Air was introduced in the calcination process, and the calcination was carried out at 800 °C for 6 h. The heating rate of the tube furnace was 2 °C·min^{-1}. Finally, the pure phase inorganic PSFO and LPSFO fibers could be obtained.

2.3. Characterization

The surface morphology of nanofibers was observed by scanning electron microscopy (SEM, Sigma 500) and transmission electron microscopy (TEM, JEOL JEM-2100 F). The phase structure of nanofibers was characterized by x-ray diffraction (XRD, TTR-III). The element distribution of the nanofibers was measured using an energy dispersive spectrometer (EDS, Hitachi S4800). The calcination of the sample was carried out in a vacuum tube furnace. A physical property measurement system (PPMS, Quantum Design) was used to characterize the electrical and magnetic properties of the calcined nanofibers.

3. Results and discussion

3.1. XRD

The phase structure analysis of PSFO and LPSFO nanofibers are characterized by XRD. The XRD patterns of PSFO and LPSFO nanofibers are shown in Fig. 1. According to the XRD pattern, it can be observed that there are no impurity peaks in the spectrum of PSFO nanofibers nor LPSFO nanofibers, indicating that the sample is a pure phase without other impurities. Furthermore, it can be seen from the pattern that the sample peaks are all relatively narrow and the peak shapes are relatively sharp, indicating that the PSFO and LPSFO nanofibers have good crystallinity and good lattice integrity. Moreover, a new diffraction peak at about 25° can be observed in the XRD pattern of LPSFO, which proves that the element of La is successfully doped.[39]

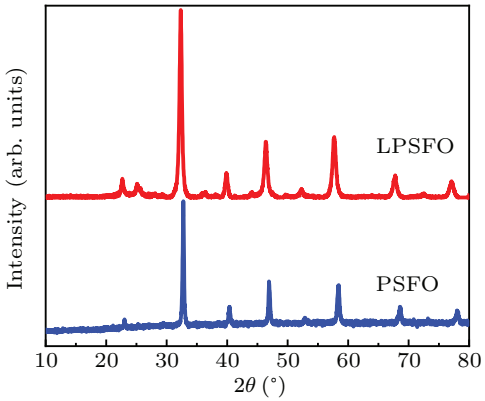


Fig. 1. XRD data of calcined PSFO and LPSFO nanofibers.

3.2. SEM and TEM

The morphology of PSFO and LPSFO nanofibers before and after calcination are analyzed by SEM and TEM images. The characterization results are shown in Figs. 2 and 3. It can be seen from the SEM images that the fiber diameter distribution of the PSFO and LPSFO nanofiber membranes prepared by the electrospinning method are relatively uniform, and the floating change of the fiber diameter is caused mostly by the unstable jet under the electric field. Nano Measurer software is used to measure the diameters of the two types of fibers, and the histograms of the diameter distribution of PSFO and LPSFO nanofibers are obtained.

According to Fig. 2(a), it can be found that the diameter distribution of PSFO/PVP composite nanofibers is mostly between 250 nm and 350 nm. Figure 2(b) shows the morphology of a single fiber, voids or particles. It can be seen from Fig. 2(c) that the calcination made the nanofibers change significantly. At high temperatures, PVP and inorganic salts are decomposed, and accompanied by the crystallization process of PSFO, the fiber surface is rougher and the fiber diameter is greatly reduced. However, the calcined PSFO nanofibers obviously have a more uniform diameter distribution. Figure 2(d) shows more clearly the morphology of a single fiber after calcination. The fiber is relatively rough and has a small diameter.

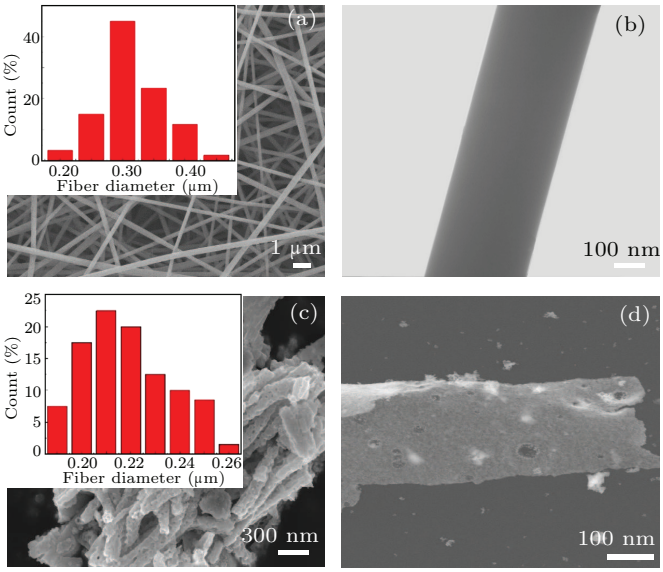


Fig. 2. (a) SEM and (b) TEM images of PSFO precursor fibers, (c) SEM and (d) TEM images of calcined PSFO fibers, with inset showing diameter distribution histogram of nanofibers.

Figures 3(a) and 3(c) show the comparison between LPSFO nanofibers before and after having been calcined. It can be observed that the diameters of LPSFO/PVP composite fibers are in a range of about 250 nm–350 nm, and the diameters of the pure phase LPSFO nanofibers after having been calcined. It is reduced by about 150 nm, and the morphol-

ogy of the fiber is changed from originally very smooth to the rough morphology after having been calcined.

Since the diameters of PSFO and LPSFO nanofibers are small after having been calcined, the electron hopping is restricted to the interior of the fiber, and the coherence length of electrons at low temperature is significantly larger than the fiber diameter. Therefore, the nanofiber can be regarded as an independent 1D structure.

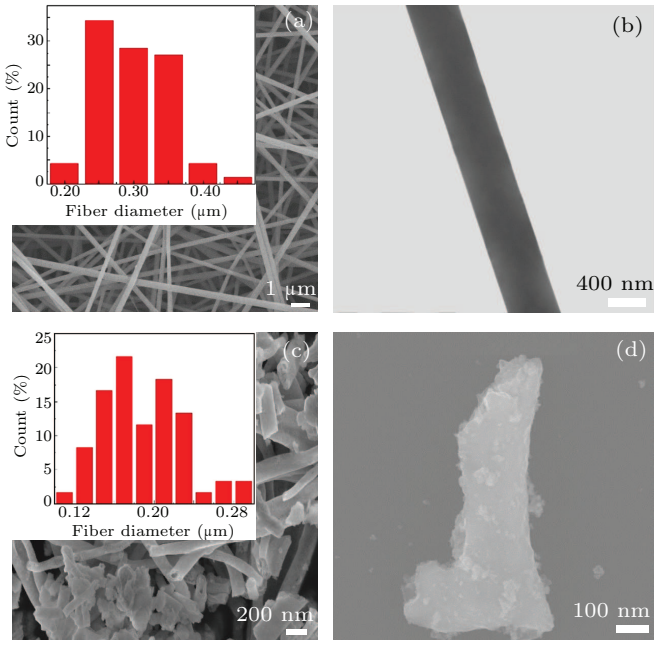


Fig. 3. (a) SEM and (b) TEM images of LPSFO precursor fibers. (c) SEM and (d) TEM images of calcined LPSFO fibers, with inset showing diameter distribution histogram of nanofibers.

3.3. EDS

Energy dispersive spectrometer (EDS) is used to qualitatively analyze the element type and element content of the material, which can more accurately determine the element composition and relative ratio of the elements in PSFO and LPSFO. As shown in Figs. 4(b)–4(e) and 5(b)–5(f), it can be observed that in the PSFO nanofibers, the Pr, Sr, Fe, and O elements are relatively uniformly distributed and there are no other elements. Similarly, in the LPSFO nanofibers, the La, Pr, Sr, Fe, and O elements are uniformly distributed and do not contain other impurity elements. In Tables 1 and 2, it can be concluded that the content values of elements are more consistent with the composition ratios of $Pr_{0.5}Sr_{0.5}FeO_3$ and $La_{0.25}Pr_{0.25}Sr_{0.5}FeO_3$, respectively.

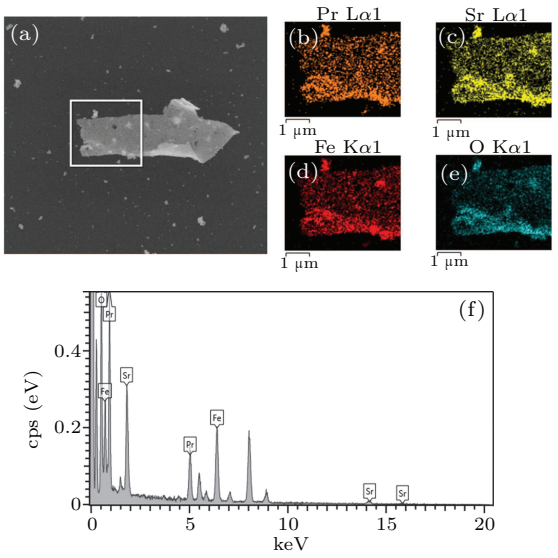


Fig. 4. (a) EDS test performed on a part of PSFO nanofibers. (b)–(e) Distribution of Pr, Sr, Fe, and O. (f) Element compositions in PSFO nanofibers.

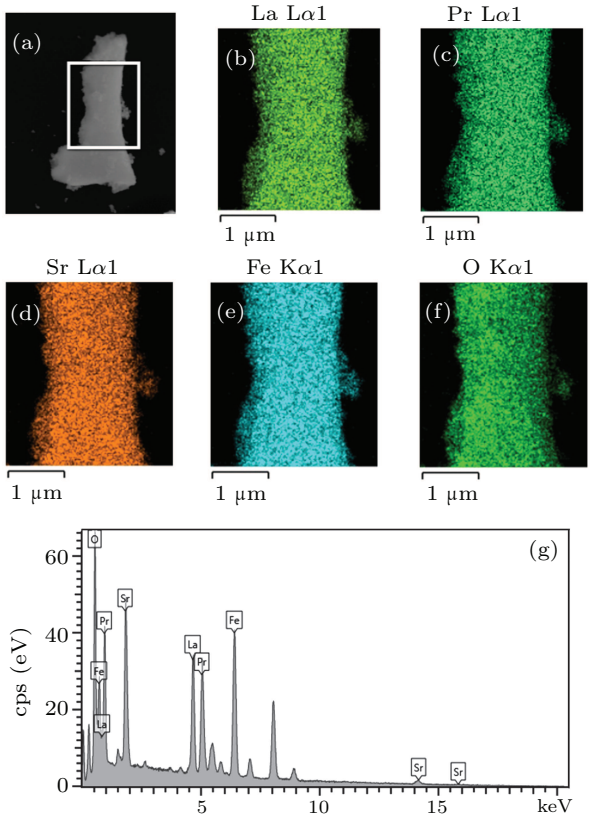


Fig. 5. (a) EDS test performed on a part of LPSFO nanofibers. (b)–(f) Distribution of La, Pr, Sr, Fe, and O. (g) Element compositions in LPSFO nanofibers.

Table 1. Composition ratios in PSFO nanofibers.

Element	Line type	wt%	wt% Sigma	Atomic percentage
O	K line	35.02	0.60	73.83
Fe	K line	21.60	0.44	13.04
Sr	L line	18.81	0.50	7.24
Pr	L line	24.57	0.50	5.88
Total		100.00		100.00

Table 2. Composition ratios in LPSFO nanofibers.

Element	Line type	wt%	wt% Sigma	Atomic percentage
O	K line	25.22	0.21	65.43
Fe	K line	21.49	0.14	15.98
Sr	L line	15.58	0.15	7.38
La	L line	24.71	0.18	7.38
Pr	L line	13.00	0.18	3.83
Total		100.00		100.00

3.4. Magnetic properties

The direct or indirect exchange between spins occurs when the intrinsic magnetic moment of the atom is not zero. This exchange action corresponds to the magnitude of the exchange energy, which changes with the positional relationship between the spins. Sometimes the parallel arrangement between adjacent spins has the lowest energy, sometimes the antiparallel arrangement possesses the lowest energy, sometimes the tilted state has the lowest energy, and sometimes the exchange interaction is too weak, and the exchange interaction between adjacent spins is destroyed by thermal disturbance. Therefore, the material exhibits different types of magnetism to the outside.

The effect of phonons makes the system enter into a disordered state, and its average energy can be expressed as $k_{\mathrm{B}}T$, that is, when the temperature is T, the energy that drives the system into a disordered state is $k_{\mathrm{B}}T$. Magnetic ordering states exhibit different properties such as ferromagnetism or antiferromagnetism. When the temperature of the material rises above the Curie temperature or the Neel temperature, the thermal motion of the phonons is greater than the magnetic interaction, and the system enters into a disordered state. It shows the characteristics of paramagnetism to the outside. Some materials are paramagnetic at room temperature, but at low temperatures, the energy of phonons becomes lower, and the exchange of magnetic moments becomes prominent, forming a ferromagnetic state or an antiferromagnetic state, or other states thereby exhibiting corresponding magnetic characteristics. In short, the exchange of spins causes an ordered state to form between the magnetic moments, while the role of phonons lies in driving the system into a disordered state. This is a pair of opposite factors, and it is also one of the reasons why we want to study magnetism changing with temperature.

In order to study the magnetic properties of PSFO and LPSFO nanofibers at low temperatures, vibrating sample magnetometer (VSM) is used to measure one of the components of PPMS. The magnetic analysis of material should be based on the magnetic structure of the material, and the magnetic structure analysis often needs to rely on high-end methods such as neutron diffraction. It has been reported in the literature that the structure of $Pr_{1-x}Sr_xFeO_{3-w}$ has been studied and calculated in detail.[43,44] Based on the above research, we conduct experimental analysis and discussion on the magnetic properties of PSFO and LPSFO nanofibers.

Figures 6(a) and 6(c) reveal the magnetization of PSFO and LPSFO nanofibers at 300 K and 10 K, respectively. Obviously, the magnetic field-magnetization curves of the two different samples are relatively smooth, showing extremely good repeatability, and at the same time, there is no step-like mutation phenomenon on the curve. When the test temperature is constant, the magnetization of PSFO and LPSFO nanofibers are both proportional to the magnetic field. Moreover, the hysteresis can be seen to exist on the M–H curve, which is a hysteresis loop. At a temperature of 10 K, there is a large ferromagnetic phase ratio inside the LPSFO, and a larger coercive force is shown on the hysteresis loop (about 1120 Oe). However, the coercive force of PSFO is smaller (about 600 Oe) than that of LPSFO when the internal ferromagnetic phase ratio is small, but both are far from their saturation magnetic fields. It can be observed that both PSFO and LPSFO have certain ferromagnetic behaviors. A basic feature of ferromagnetic properties is hysteresis. To put it simply, the hysteresis phenomenon is that when the magnetic material is magnetized, the magnetization of the material dose not decrease simultaneously in the process of reducing the external magnetic field, but it gradually decreases until the reverse magnetic field is applied, and finally reaches a saturation state in the reverse direction. Therefore, the magnetization curve of the up-field direction and that of down-field direction do not coincide, and there is a hysteresis between them. In addition, when the intensity of the applied magnetic field is low and the test temperature is 10 K, the magnetic susceptibility of PSFO and LPSFO nanofibers significantly exceed the magnetic susceptibility measured at 300 K. The reason for the above external performance can be attributed to the gradual melting of the ordered phase of the charge, so the portion of the ferromagnetic phase is greatly increased. In addition, the higher iron concentration can also result in Fe–O–Fe superexchange. The PSFO and LPSFO nanofibers both have higher content of iron, but according to the ferromagnetism shown in the above figure, it can be concluded that the Fe–O–Fe exchange effect contained is weak, or it can be understood as a part of the higher-order superexchange iron effect. Moreover, it can be observed from Figs. 6(a) and 6(c) that when the external magnetic field reaches 3 T or even 5 T, the magnetization of neither PSFO nor LPSFO is saturated. Therefore, as the external magnetic field increases, the ratio of magnetization to ferromagnetic phase continues to increase. The size effect and large specific surface area of nanofibers trigger off these phenomena. It also shows that the ferromagnetic phase-portion in PSFO and in LPSFO are both relatively low, which cannot cause the magnetization to reach the saturation level. However, under the same external magnetic field, PSFO and LPSFO nanofibers show greater magnetization at low temperatures, indicating that at low temperatures, PSFO and LPSFO nanofibers contain a higher portion of ferromagnetic phase.

Figures 6(b) and 6(d) show the temperature-dependent FC and ZFC curves of PSFO and LPSFO nanofibers under magnetic fields of 3 T and 0.1 T, respectively. The FC curve and ZFC curve of PSFO nanofibers are separate from each other at 180 K. When the temperature drops below 180 K, the ferromagnetic phase gradually appears due to the freezing of

the magnetic moment, but due to the low phase portion of the ferromagnetic inside the PSFO nanofibers, the FC and ZFC curves are not overlapped. The sharp peaks on the ZFC curve are not obvious. Comparing with the sample of PSFO powder, the sharp point on the ZFC curve of the PSFO nanofiber appears at a lower temperature point, which means that it has a lower spin glass transition temperature, and the FC and ZFC curves are not completely separate from each other. Both indicate that the ferromagnetic phase inside the PSFO nanofibers is lower than that of the PSFO powder.

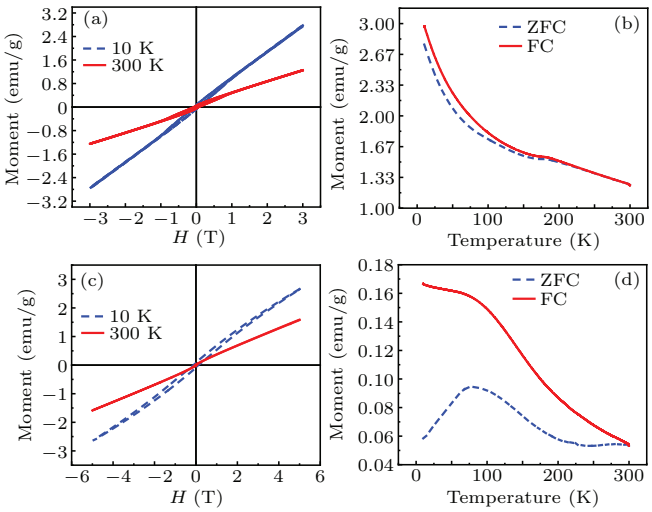


Fig. 6. (a) Magnetization of calcined PSFO nanofibers at 10 K and 300 K, (b) the curves of FC and ZFC *versus* temperature under magnetic field of 3 T, (c) the magnetization of calcined LPSFO nanofibers at 10 K and 300 K under magnetic field of 5 T, and (d) curves of FC and ZFC *versus* temperature under magnetic field of 0.1 T.

For the LPSFO nanofibers, as the temperature decreases, the FC and ZFC curves are always in a separate state, and the ZFC curve has an obvious peak at 75 K. Based on this image, it can be concluded that the blocking temperature T_B of the LPSFO nanofibers is around 75 K. When the temperature is lower than T_B, the phase separation region of LPSFO nanofibers is frozen to form a spin glass state. When the temperature exceeds T_B, the magnetic moment is thawed and can rotate freely. For the LPSFO nanofiber, the magnetic system after ZFC is isolated, so the magnetic susceptibility becomes lower. Therefore, the appearing of the frozen phase is due to the competition between the ferromagnetic phase and the antiferromagnetic phase. In the magnetic measurement, the overall magnetism of LPSFO nanofibers is tested. The contribution of antiferromagnetic relative to magnetization is very small, and it do not affect the overall magnetism of LPSFO nanofibers.

It can be seen directly in Fig. 6 that under the same temperature and the same external magnetic field, the magnetization of PSFO nanofibers is significantly higher than that of LPSFO. However, the LPSFO has a more obvious hysteresis loop, and at the same time shows a more obvious ferromagnetic behavior in the FC and ZFC curves. The above phenomena can be attributed to the influence of La element on the entire magnetic system. Moreover, although it leads the overall magnetization of the material to decrease, it can be observed that the incorporation of La element increases the ferromagnetic ratio of the sample.

3.5. Electrical performance

For testing the electrical properties of PSFO and LPSFO nanofibers, the electronic transport option of PPMS is used to test mainly the temperature-dependent resistance curves of PSFO and LPSFO nanofibers. As shown in Figs. 7(a) and 7(c), the temperature dependence of the resistance of the PSFO and LPSFO nanofibers are measured. In the tests of both samples, a significant metal–insulator transition can be found. When the temperature decreases, the resistance of PSFO and LPSFO nanofibers gradually increase, showing obvious semiconductor behavior. As the temperature continues to decrease, the ferromagnetic metal phase gradually infiltrates, and the PSFO and LPSFO nanofibers undergo metal insulator transformation at the transition temperature of $T_{IM} \approx 110$ K and $T_{IM} \approx 180$ K, respectively. Owing to the doping of La element, LPSFO nanofibers have a higher ferromagnetic phase portion than PSFO nanofibers. Therefore, the metalinsulator transition temperature of LPSFO is higher than that of PSFO. Below the transition temperature, the resistance decreases as the temperature decreases, and in turn exhibits metallic behavior. For the semiconductor behavior before the transition of the metal insulator, the Mott's variable-range hopping (VRH) model can describe the electronic conduction model. In this model, the dependence of the resistivity $\rho(T)$ on the temperature T is as follows:

$$\rho(T) = \rho_0 \cdot \exp(T_0/T)^{1/(1+n)}, \tag{1}$$

$$T_M = 18/k_B L c^3 N(E_F), \tag{2}$$

$$R_{hop} = (3/8)(T_M/T)^{1/4} Lc, \tag{3}$$

after simplifying the calculation of the above formula, the formula can be obtained as follows:

$$\ln \rho(T) \propto T^{-1/(n+1)}, \tag{4}$$

where ρ is a constant, when the dimensions of the model are 1, 2, and 3, n in the formula is equal to 1, 2, and 3, respectively; T_0 is the Mott characteristic temperature, describing the energy barrier that electrons need to overcome when hopping from one local state to another. The fitted results of PSFO and LPSFO nanofibers above the transition temperature with the 1D VRH model are shown in Figs. 7(b) and 7(d). It can be observed that as the temperature decreases, the resistance increases exponentially, which is a characteristic of semiconductor materials. It is reasonable to use the 1D Mott's VRH model to describe the conduction mechanism of PSFO and LPSFO nanofibers.

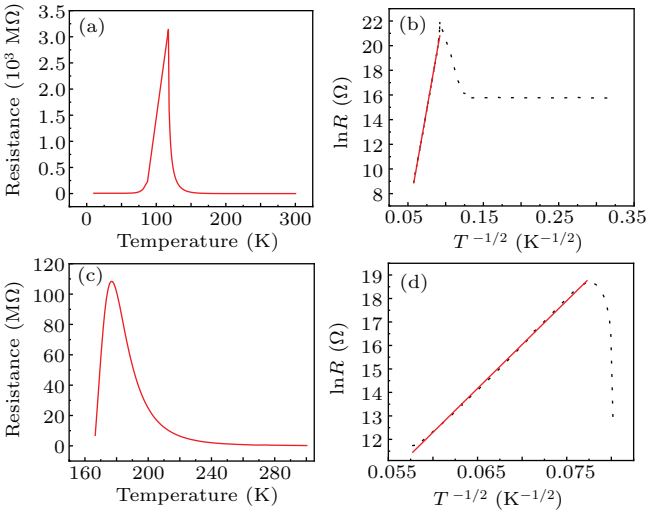


Fig. 7. (a) The *R*–*T* curve of PSFO nanofibers, and (b) 1D VRH fitting of the curve. (c) The *R*–*T* curve of LPSFO nanofibers, and (d) 1D VRH fitting of the curve.

4. Conclusions

The PSFO and LPSFO nanofibers are fabricated by electrospinning method followed by high-temperature calcination. Material characterizations prove that the samples are pure and free of impurities. The magnetic results show that both PSFO and LPSFO nanofibers have a certain portion of ferromagnetic phase. With temperature decreasing, PSFO and LPSFO nanofibers undergo a significant transition to a spin-glass state. Moreover, the doping of La element has an influence on the system. Although it leads the overall magnetization intensity of the material to decrease, it makes the ferromagnetic ratio of the sample higher. The temperature-dependent resistance curves prove that the PSFO and LPSFO nanofibers have both a metal–insulator transition as the temperature decreases. For the high-temperature semiconductor behavior of the nanofibers, the dependence of the resistance on temperature can be explained by 1D Mott's VRH model, which reflects the influence of the mesoscopic structure on the electronic transport mechanism.

Acknowledgements

Project supported by the National Natural Science Foundation of China (Grant Nos. 51973100 and 11904193), the Fund from the State Key Laboratory of Bio-Fibers and Eco-Textiles, Qingdao University, China (Grant No. RZ2000003334), and the National Key Research and Development Project, China (Grant No. 2019YFC0121402).

References

[1] Yang Z G G, Stevenson J W and Singh P 2003 *Adv. Mater. Process* **161** 34
[2] Lu J B, Zhang Z T and Tang Z L 2005 *Rare Metal Mat. Eng.* **34** 1177
[3] Lenka R K, Patro P K, Patel V, Muhmood L and Mahata T 2021 *J. Alloys Compd.* **860** 158490
[4] Hu X, Xie Y, Wan Y, Yang Y, Wu X and Xia C 2021 *Appl. Catal. B-Environ.* **286** 119901
[5] Vivanpatarakij S, Assabumrungrat S and Laosiripojana N 2007 *J. Power Sources* **167** 139
[6] Steele B C H and Heinzel A 2001 *Nature* **414** 345
[7] Strazza C, Del Borghi A, Costamagna P, Gallo M, Brignole E and Girdinio P 2015 *Energ. Convers. Manage.* **100** 64
[8] Pelegrini L, Rodrigues Neto J B and Hotza D 2016 *Rev. Adv. Mater. Sci.* **46** 6
[9] Reddy A A, Tulyaganov D U, Kharton V V and Ferreira J M F 2015 *J. Solid State Electr.* **19** 2899
[10] Lyu Y, Wang F, Wang D and Jin Z 2020 *Mater. Technol.* **35** 212
[11] Lee Y H, Chang I, Cho G Y, Park J, Yu W, Tanveer W H and Cha S W 2018 *Int. J. Precis Eng Manuf-Green Technol.* **5** 441
[12] Benamira M, Ringuede A, Hildebrandt L, Lagergren C, Vannier R N and Cassir M 2012 *Int. J. Hydrogen Energy* **37** 19371
[13] Zhu B 2009 *Int. J. Energ. Res.* **33** 1126
[14] Timurkutluk B, Timurkutluk C, Mat M D and Kaplan Y 2011 *Int. J. Energ. Res.* **35** 1048
[15] Ozmen O, Zondlo J W, Lee S, Gerdes K and Sabolsky E M 2016 *Mater. Lett.* **164** 524
[16] Ziemann P and Khokhlov A R 2013 *Beilstein J. Nanotech.* **4** 678
[17] Yu F and Di L 2020 *Nanomaterials* **10** 333
[18] Chen C, Fan Y, Gu J, Wu L, Passerini S and Mai L 2018 *J. Phys. D: Appl. Phys.* **51** 113002
[19] Shao H 2017 *Energies* **10** 1767
[20] Nesaraj A S 2010 *J. Sci. Ind. Res.* **69** 169
[21] Ishihara T 2016 *J. Korean Ceram. Soc.* **53** 469
[22] Hao S J, Wang C, Liu T L, Mao Z M, Mao Z Q and Wang J L 2017 *Int. J. Hydrogen Energ.* **42** 29949
[23] Fan L, Zhu B, Su P C and He C 2018 *Nano Energy* **45** 148
[24] Fabbri E, Bi L, Pergolesi D and Traversa E 2012 *Adv. Mater.* **24** 195
[25] Medvedev D A, Lyagaeva J G, Gorbova E V, Demin A K and Tsiakaras P 2016 *Prog. Mater. Sci.* **75** 38
[26] Hossain S, Abdalla A M, Jamain S N B, Zaini J H and Azad A K 2017 *Renew. Sust. Energ. Rev.* **79** 750
[27] Zhu Z, Guo E, Wei Z and Wang H 2018 *J. Power Sources* **373** 132
[28] Shimada H, Yamaguchi T, Sumi H, Yamaguchi Y, Nomura K and Fujishiro Y 2018 *Ceram. Int.* **44** 3134
[29] Huan D, Shi N, Zhang L, Tan W, Wang W, Xia C, Peng R and Lu Y 2018 *ACS Appl. Mater. Interfaces* **10** 1761
[30] Wang B, Bi L and Zhao X S 2018 *Ceram. Int.* **44** 5139
[31] Chen Y, Yoo S, Pei K, Chen D, Zhang L, *et al.* 2018 *Adv. Funct. Mater.* **28** 1704907
[32] Choi S, Kucharczyk C J, Liang Y G, Zhang X H, Takeuchi I, Ji H I and Haile S M 2018 *Nat. Energy* **3** 202
[33] Hou J, Miao L, Hui J, Bi L, Liu W and Irvine J T S 2018 *J. Mater. Chem. A* **6** 10411
[34] Yamaura H, Ikuta T, Yahiro H and Okada G 2005 *Solid State Ionics* **176** 269
[35] Sun W, Zhu Z, Jiang Y, Shi Z, Yan L and Liu W 2011 *Int. J. Hydrogen Energy* **36** 9956
[36] Peng R, Wu T, Liu W, Liu X and Meng G 2010 *J. Mater. Chem.* **20** 6218
[37] Fabbri E, Bi L, Tanaka H, Pergolesi D and Traversa E 2011 *Adv. Funct. Mater.* **21** 158
[38] Grimaud A, Mauvy F, Bassat J M, Fourcade S, Rocheron L, Marrony M and Grenier J C 2012 *J. Electrochem. Soc.* **159** B683
[39] Ma J, Tao Z, Kou H, Fronzi M and Bi L 2020 *Ceram. Int.* **46** 4000
[40] Nowik I F I and Awana V P S 1999 *J. Magn. Magn. Mater.* **192** 67
[41] Zhu W, He J, Ti R, Jin Y, Xu T, Yue C, Huang F, Lu X and Zhu J 2014 *Phys. Status Solidi A* **211** 2833
[42] Chen C C, Xu Z C and Ying X N 2016 *Solid State Commun.* **228** 27
[43] Brinks H W, Fjellvag H, Kjekshus A and Hauback B C 2000 *J. Solid State Chem.* **150** 233
[44] Stange M, Linden J, Kjekshus A, Binsted N, Weller M T, Hauback B C and Fjellvag H 2003 *J. Solid State Chem.* **173** 148